PROCEEDINGS OF SCIENCE

Time profile of fluorescence in organic scintillator out to 10 microseconds

S. Nutter *†[1], T. Anderson[2], Y. Chen[2], S. Coutu[2], T. LaBree[1], J.T. Link[3], J.W. Mitchell[4], S.I. Mognet[2], K. Wallace[1], M. Yu[2]

[1]Dept. Of Physics, Geology, & Engineering Technology, Northern Kentucky University, Highland Heights, KY, 41076 USA
[2]Dept. of Physics, Penn State University, University Park, PA 16802, USA
[3]Center for Research and Exploration in Space Science and Technology (CRESST) UMBC, Baltimore MD, 21250, USA
[4]Astroparticle Physics Laboratory, NASA Goddard Space Flight Center, Greenbelt, MD 20771, USA

A technique to identify energetic cosmic-ray electrons in the face of large nuclei backgrounds is to use a calorimeter followed by a shower tail-catcher boron-doped scintillator on a balloon or satellite instrument. Thermalized neutrons produced in interactions of the cosmic ray within the material of the instrument can be detected at late times (several microseconds) following the triggering event. To this end, for example, the DAMPE satellite instrument includes a Neutron Detector at the bottom of its instrument stack, and the ISS-CREAM space station experiment similarly includes a Boronated Scintillator Detector. One difficulty of interpreting the thermal neutron capture signal in the scintillator is that a late fluorescence signal is also present, with time scales similar to those of the 2.7 microsecond exponentially falling neutron capture time distribution. Thus the two effects must be carefully disentangled.

We have measured the response of a non-boronated thick scintillator to electron and pion showers in CERN beam tests, and find the presence of a significant late fluorescence component in the light yield that must be accounted for. The measured scintillator response is well represented by a three component yield model, with time constants from ~10 ns to ~2.4 microseconds and appropriate relative strengths. GEANT4 was modified to accommodate this three-component scintillation model, yielding excellent agreement with the CERN beam test data. We describe the measurements and the model in this work.

36th International Cosmic Ray Conference -ICRC2019-
July 24th - August 1st, 2019
Madison, WI, U.S.A.

* Speaker
† Email: scott.nutter@nku.edu

PoS(ICRC2019)115

1. Introduction

A common tool in elementary particle detection is the organic scintillator. Such scintillators are often made by doping polyvinyltoluene plastic with a primary scintillator chemical and a secondary fluor to act as a waveshifter [1-2], shifting the typically deep UV scintillation light to wavelengths more easily detected by standard devices utilizing the photoelectric effect, such as the photocathodes on photomultiplier tubes. Compared to inorganic detectors (crystals and liquefied noble gases, such as BaF, NaI(Tl), or liquid Ar), plastic scintillators are inexpensive, easily machined, and have low density. The common use for plastic scintillators takes advantage of their fast (few ns) rise time and similar decay time. This signal arises from fluorescence due to the decay of excited singlet states in the scintillator. Additional signal may result due to the slower process of phosphorescence from metastable triplet states with a time scale on the order of as much as a millisecond (or even longer), or from delayed fluorescence due to shifting of energy from the metastable states back to the fluorescing states [3]. Typically, the late component of the scintillator yield is very small relative to the early component, and is ignored in single particle applications due to a short window of signal integration and/or a focus on the timing aspect of the signal. However, in applications which look at long times after the initial signal, or with high rates, in which any late signal may still be present when a following trigger occurs, the late component of the scintillator signal must be taken into account. For example, in neutron detection in neutron spectroscopy [4], homeland security applications [5], and in searches for long-lived particles (e.g., dark matter), signals may be integrated out to several microseconds (e.g., [6]).

The present study is motivated by the use of a boron-loaded Eljen EJ-254 plastic scintillator on the ISS-CREAM experiment [7], and is described in detail in [8] and [9]. The neutron content of showers initiated by leptons (e.g., electrons or positrons) differs from that of showers initiated by hadrons (e.g., protons or nuclei). The ISS-CREAM Boronated Scintillator Detector (BSD) is designed to determine the neutron content of cosmic-ray initiated particle showers (generated in the ISS-CREAM carbon targets and calorimeter structure) after neutron thermalization and capture in the scintillator. Our goal is to successfully reproduce beam test measurements with GEANT4-based simulations in order to interpret flight data. In characterizing the performance of the EJ-254 BSD in pion and positron beams at CERN in 2012, we noticed that the amount of late light collected exceeded that predicted by GEANT4 [10] simulations by a factor of 30 [11]. These simulations used the standard G4Scintillation object with the parameters (e.g., rise time, fall time, yield) entered for EJ-254 as given by the manufacturer. As a result, we chose to measure the late light (sometimes referred to as "afterglow" in the literature) using showers from particle beams to excite the fluors in the plastic, rather than more typical methods involving UV light or gamma particles, in order to more closely reproduce the eventual use case of the scintillator material in the ISS-CREAM experiment placed below a calorimeter [7]. In addition, due to the details of the electronics used in the BSD, we focused on the value of the integrated signal at short times (< 500 ns) and mapped out the detailed response for times > 1 μs.

The base scintillator for the EJ-254 is the EJ-200 [12], a fast, high yield, general purpose and widely used plastic scintillator (similar to Bicron/Saint-Gobain BC-408 and Nuclear Enterprise's Pilot F). EJ-200 uses a polyvinyltoluene scintillator doped with proprietary waveshifting fluors. Since the scintillator composition is commercially protected and not publically available, we can characterize its performance but not model it theoretically.

2. Experimental setup and results

2.1 Instrumentation

The detector used in these tests is a prototype for the Boronated Scintillator Detector (BSD) in the ISS-CREAM experiment on the ISS, with the replacement of the boronated scintillator (EJ-254) with a standard unboronated plastic scintillator, EJ-200. The scintillator is viewed by 18 photomultiplier tubes (PMTs), as described in detail in [9]. Of these, two are continually active and view the potentially bright light signal from showering particles exiting the bottom of the calorimeter, and act as trigger PMTs to initiate the rapid activation of the remaining 16 PMTs, which are kept in a quiescent state until triggered. These latter units integrate the late scintillation activity and any neutron captures in the BSD in ISS-CREAM. Thus, the BSD has two paths for signal processing: one associated with the large signals due to the primary shower, and a second associated with small signals due to late light from neutron captures and delayed fluorescence.

The BSD prototype used for the 2016 CERN beam test described here consisted of a 60 cm × 60 cm × 3.8 cm monolithic slab of EJ-200 scintillator viewed by 10 Hamamatsu R1924A PMTs [13], which have a rise time of 1.5 ns and a spectral response similar to the spectral output of the EJ-200. Two of these ("early light" PMTs) were outfitted with low-gain resistor chains, were always sensitive to light, and were used as triggers for the other eight PMTs ("late light" PMTs). The large signals created by showers cause significant afterpulsing in the high gain, late light PMTs if they were active at the time of the incident particle shower. Thus the other eight were instead kept in an inactive, quiescent state of zero gain, in which photoelectrons were not multiplied. This was accomplished by reversing the voltage on the PMTs' first two dynodes until after the shower pulse was completed and triggered the active, early-light PMTs [14]. A trigger from a shower started the process of ramping up the voltage on these two dynodes, making these tubes sensitive and stable after a period of about 400 ns. These tubes were then used to integrate the light signal occurring long (1-10 μs) after the initial particle shower.

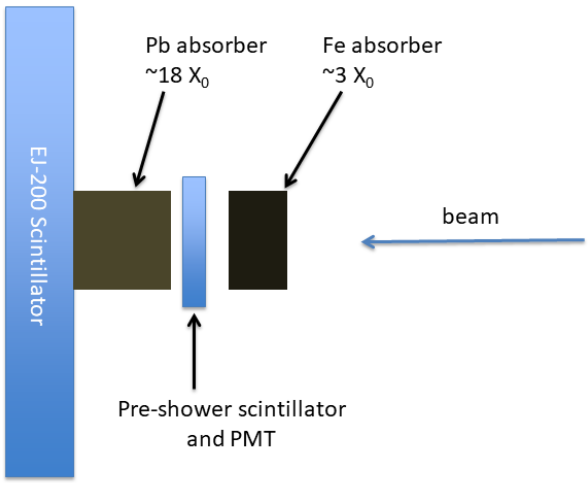

Fig. 1. Schematic layout of the 2016 CERN beam tests, not to scale.

The data digitization electronics integrated the individual PMT signals in a specified, adjustable time window. We used a consistent effective window of 0 – 400 ns to integrate the trigger PMTs, and a window ranging in width and start time from as early as one μs after the trigger to as late as 50 μs. The electronics had low and high digitization gain channels and were capable of distinguishing the single photoelectron peak for the late-light PMTs. An event consisted of the digitized signal from all ten PMTs.

Tests with this prototype instrumentation had been performed at CERN in positron and pion test beams in November 2012 using the EJ-254 boronated scintillator, followed by additional beam tests at CERN in 2015 and 2016 with an undoped EJ-200 scintillator slab of the same dimensions, and in the laboratory with atmospheric muons, and red and UV LEDs. Results from the 2012 beam test were described in [9], so that here we focus primarily on the 2016 test results, assessing the delayed fluorescence signal without a neutron capture enhancement.

2.2 CERN test beam measurement and results

The 2016 CERN test beam setup is shown in Fig. 1. The undoped EJ-200 slab was placed perpendicular to and centered on the horizontally entering beam. A combination of lead and iron absorbers (of thickness 18 and 3 radiation lengths, respectively) was placed in front of the scintillator to initiate particle showers. A pre-shower counter, consisting of a small piece of EJ-200 scintillator viewed by a Photonis XP2020 PMT, was placed between the lead and iron to identify events for which a shower started early in the absorber material. This reproduced the expected operating mode in the ISS-CREAM instrument, and ensured that a sufficiently mature shower entered the large plastic scintillator to produce the brighter light signals leading to easily detectable late fluorescence-light levels.

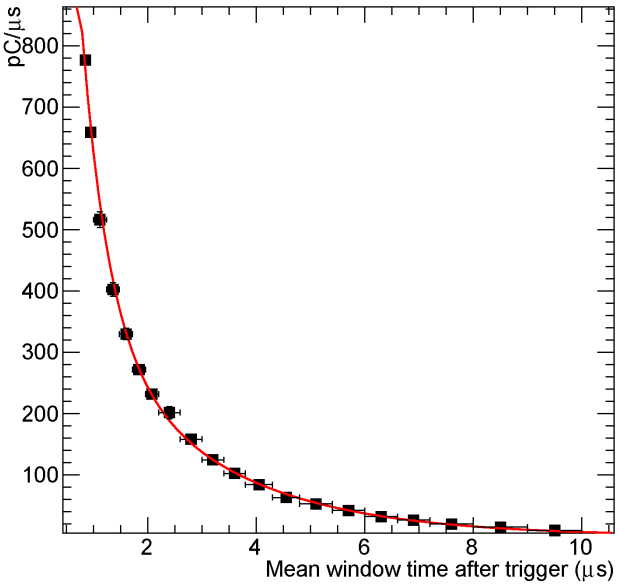

Fig. 2. The measured signal in the EJ-200 scintillator from 1 to 10 μs from an electron-induced shower at a depth of ~21X_0 (following lead and iron absorbers). The curve is a two-component exponential fit, as described in the text.

We ran a variety of beam tests at CERN with five different late-light PMT operating voltages. Electron momenta of 50 – 250 GeV/c were sampled in steps of 50 GeV/c, and a fixed pion momentum of 300 GeV/c was also available. A beam stop, which absorbed the incident positrons and pions, produced penetrating muons, which were used to provide response calibration for single minimum-ionizing particles (MIPs). Raw signals were pedestal-subtracted, converted to charge units (Coulombs), then normalized by the single muon response.

The relative response of the scintillator at times between 1 and 10 μs was obtained in pC/μs units (Fig. 2), in time windows with sizes ranging from 100 ns to 1 μs. We did not observe measurable signals beyond 10 μs after the initial particle showers. A single exponential function proved a poor fit, while a two-exponential fit (shown) agreed with the data very well (see Section 3).

2.3 Muon and LED tests and results

The muon and LED tests were conducted with the non-boronated EJ-200 scintillator slab in an institutional physics laboratory using the same PMTs and high voltages as in the CERN beam tests. The instrument was placed horizontally on a lab bench and allowed to self-trigger on cosmic-ray muons incident anywhere on the scintillator. Early-light PMT signals were consistently integrated from 0 – 400 ns, and late-light PMT signals were integrated in a 0 – 400 ns window to calibrate their muon response, and separately in the window 900 ns – 5900 ns to quantify the late-light delayed fluorescence component. Clear muon-induced signals were seen for each PMT in the early window as well as in the late window. An average of 105 pe/PMT were detected [15]. The single pe dark-noise rate in a given PMT was about 500 Hz.

We checked that the observed late light in this test was not due to something other than fluorescence in several ways. First, we triggered the scintillator readout at a fixed rate (randomly relative to muon arrivals) and verified that there was no unexpected early or late signal other than electronics pedestal. We also used a red LED (Kingbright model WP424SRDT, with a peak wavelength of 655 nm) tuned to a brightness approximating that of a muon in the early channel and looked for light in the late channel. None was present, so that at the wavelength of the red LED the scintillator's atomic and/or molecular states responsible for delayed fluorescence were not activated, thus verifying that the observed late light after showers was not due to the PMT or electronics. We switched out the red LED for a UV LED (Bivar Inc. model UV3TZ-395-30), with peak emission output at 395 nm, and now did find a measurable late signal resulting from exciting the primary scintillator and/or waveshifting fluors.

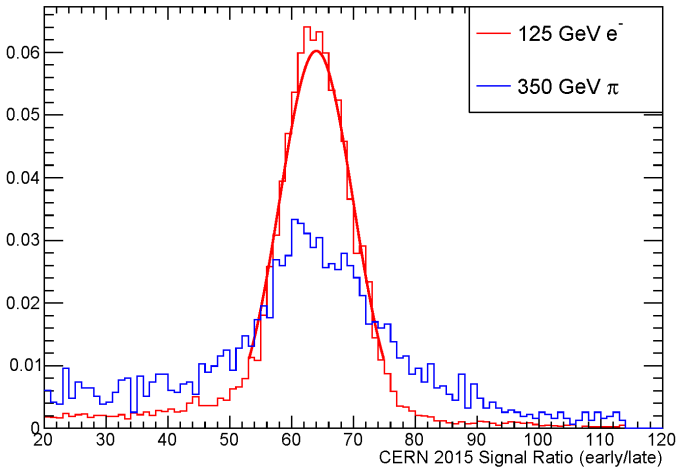

Fig. 3. Ratio of early-to-late scintillation light signals measured with electron and pion beams at CERN in 2015. A Gaussian curve fit to the peak of the electron signal ratio distribution yields the parameter *R* used in developing the scintillation model as described in the text. Distributions are normalized to unit area.

3. Scintillation yield model

To take advantage of the GEANT4 scintillation code, we developed a model of the light yield based on multiple components, each with an exponential shape. The existing GEANT4 model has two components (fast and slow), with a common rise time. We modified the GEANT4 code to add a third exponential component (medium). Our measurements are focused on times greater than 1 μs (medium and slow) in comparison with the integrated signal in the first 400 ns (fast). The model assumes that the rise times of all three components are equal. Since we only performed detailed measurements of the scintillator response at times greater than 900 ns after excitation, we would recommend only using the detailed model shape at times greater than 1 μs, the earliest time at which we measured the late light. Also, the model should be valuable in

predicting relative afterglow levels past ~1 μs, since we tuned the model to the relative amounts of integrated early and late light.

We characterize the scintillation yield as a function of time, *Y(t)*, in photons or photoelectrons per second, produced by the EJ-200 slab as

$$Y(t) = \sum_{i=1}^{3} N_i \left(\frac{a+\tau_i}{\tau_i^2}\right)\left(1-e^{-\frac{t}{a}}\right)\left(e^{-\frac{t}{\tau_i}}\right) = N\left(1-e^{-\frac{t}{a}}\right)\left[be^{-\frac{t}{c}} + d\left(e^{-\frac{t}{g}} + he^{-\frac{t}{m}}\right)\right]$$

where three components are assumed, all with a common rise time. Here,

N_i = yield of the ith component in photons per energy deposited,
N = overall yield in photons per energy deposited,
a = rise time shared by all components,
b = a measure of the relative amount of fast component to total yield,
c = fast component fall time constant,
g = medium component fall time constant,
m = slow component fall time constant,
d = a measure of the relative amount of medium and slow component to total yield,
h = a measure of the relative amount of slow component to slow plus medium yield.

Most of these values are measured directly. From lab tests using an XP2020 PMT, a small piece of EJ-200 scintillator, and a ^{60}Co radioactive source, the fast rise time was found to be a = 1.2 ns and fast fall time c = 7.8 ns. Both the rise and fall times are longer than the EJ-200 manufacturer's values of 0.9 ns and 1.2 ns, likely due to a folding in of the PMT response. From Fig. 2 we identify h = (0.192±0.089), g = (490±140) ns, and m = (2370±240) ns.

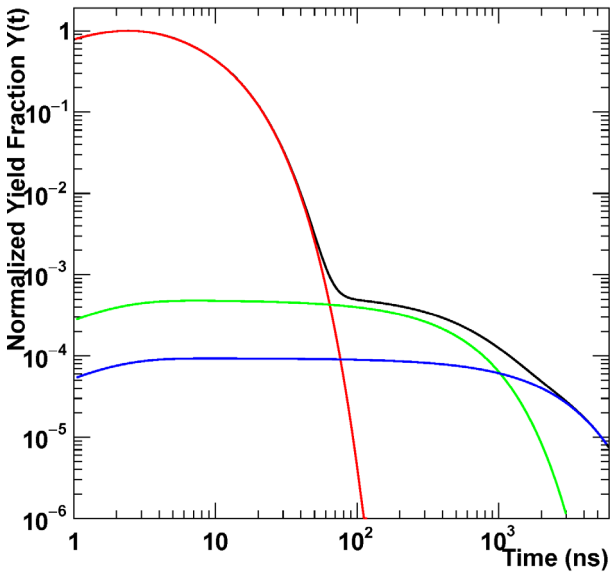

Fig. 4. The time-dependence of the EJ-200 scintillation yield model with parameters based on measurements. Curves from top to bottom as shown along the left axis of the graph: total output, fast component, medium component, and slow component. The maximum of the total output curve is normalized to one.

The constants d and b remain to be found. From a separate beam test that had been conducted at CERN in 2015 using the same scintillator as in 2016, the ratio of early-to-late light R = 64 was determined by using beam stop muon data to normalize the signals from the individual PMTs. The measured distribution of the early/late light ratio is shown in Fig. 3 for both incident electrons and pions, where the integration windows were 0-1400 ns for the trigger PMTs (early light) and 900 ns – 5900 ns for the late-light PMTs. (These window times account for the 100 ns delay imposed on the signal relative to time zero for the electronics.) Note R is a ratio of MIPs/PMT. Integrating *Y(t)* provides an expression that can be used to determine the ratio $d/b = 3.1\times10^{-4}$. A measurement of the yield in photons or photoelectrons for a specific time period provides the overall normalization N.

Thus the yield can now be expressed as

$$Y(t) = \left(1 - e^{-\frac{t}{1.2}}\right)\left[0.142e^{-\frac{t}{7.8}} + 4.4 \times 10^{-5}e^{-\frac{t}{490}} + 8.4 \times 10^{-5}e^{-\frac{t}{2370}}\right]$$

where time t is in ns. As a cross-check, note that $\frac{\int_0^{1400} Y(t)dt}{\int_{900}^{5900} Y(t)dt} = 64$, as required.

The GEANT4 G4Scintillation object code was modified to include a third exponential component. GEANT4 requires the fraction of the total yield that goes into each component. With this model, one can identify the relative total normalized yields for each component to use in simulations: fast = 95.8%, medium = 2.2%, slow = 2.0%. The early and late signals with components are shown in Fig. 4. Other parameters used in the modified GEANT4 G4Scintillation object initialization include digitizations of the manufacturer's curves for EJ-200 absorption length and the relative yield of the fast scintillation component as a function of photon energy, and a constant refractive index (n = 1.58). Note that the fast scintillation relative yield curve was also used for the medium and slow components.

These parameters were used in simulations with GEANT4 of the 2015 beam tests with the calorimeter present in front of the EJ-200 BSD prototype. Results comparing data and simulations are shown in Fig. 5. Beam particles showered in the calorimeter and passed through the BSD prototype, exciting the scintillator. Late fluorescence was measured using the parameters detemined from the 2016 beam tests with lead and iron instead of the calorimeter as described above. The overall response of the scintillator is normalized to the 125 GeV electron peak, then applied to the pion data. Agreement is excellent.

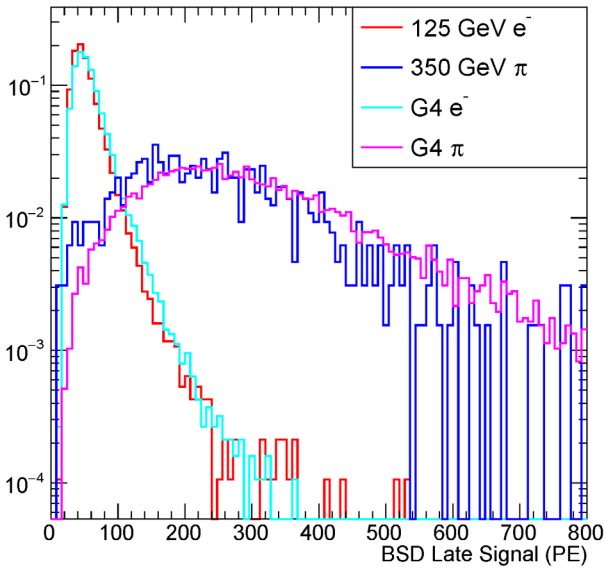

Fig. 5. For 350 GeV pion and 125 GeV electron events from the 2015 beam test leaving a similar energy deposit in the calorimeter, the integrated late activity (in photoelectrons) in the EJ-200 scintillator BSD prototype is shown for the electrons and pions for the data and GEANT4 simulations which use the late fluorescence model presented. The areas of the curves are each normalized to one.

4. Conclusion

These measurements are in agreement with previous measurements of the light output of stilbene [16], but a previous measurement in plastic scintillator at these long time scales [17] indicated that the late-light component is too small to be relevant to applications in particle physics, although a recent measurement [4] indicates light emitted at the level of ≈3×10^{-5} of the peak output at 3.0 μs. The new measurements presented here indicate consequences to using plastic scintillator in shower detectors with high rates, or applications where signal measurements extend into the several microsecond range and longer, such as dark matter searches or neutron detectors in which a charged particle passes through the scintillator.

References

[1] S.W. Moser, W.F. Harder, C.R. Hurlbut, and M.R. Kusner, *Principles and Practice of Plastic Scintillator Design*, *Radiat. Phys. Chem.* 41 (1993) 31–36.

[2] G.H.V. Bertrand, M. Hamel and F. Sguerra, *Current Status on Plastic Scintillators Modifications*, *Chem. Eur. J.* 20 (2014) 15660-15685.

[3] G.F. Knoll, *Radiation Detection and Measurement, 4th ed.* Wiley, New York NY 2010.

[4] R. Lauck, M. Brandis, B. Bromberger, V. Dangendorf, M.B. Goldberg, I. Mor, K.Tittelmeier, and D. Vartsky, *Low-Afterglow, High-Refractive-Index Liquid Scintillators for Fast-Neutron Spectrometry and Imaging Applications, IEEE Trans. Nucl. Sci.* 56 (2009) 989-993.

[5] K.D. Rakes, *Evaluating The Response Of Polyvinyl Toluene Scintillators Used In Portal Detectors*, M.S. Nuclear Engineering Thesis, Air Force Institute of Technology (2008) https://apps.dtic.mil/dtic/tr/fulltext/u2/a483290.pdf

[6] P.A. Amaudruz et al., *Design and construction of the DEAP-3600 dark matter detector*, *Astropart. Phys.* 108 (2019) 1-23.

[7] Y. Amare et al., ISS-CREAM Collaboration, *The Cosmic Ray Energetics And Mass Instrument on the International Space Station (ISS-CREAM)*, to be submitted to *JINST* (2019).

[8] S. Nutter, Y. Amare, T. Anderson et al., *Measurement of light yield of particle scintillation in plastic scintillator from one to ten microseconds, Nucl. Inst. and Meth. A* (2019) 162368, https://doi.org/10.1016/j.nima.2019.162368.

[9] Y. Amare et al., ISS-CREAM Collaboration, *The Boronated Scintillator Detector of the ISS-CREAM Experiment,* submitted to *Nucl. Inst. and Meth. A* (2019).

[10] S. Agostinelli et al., *Geant4 - a simulation toolkit, Nucl. Inst. and Meth. A* 506, 250 (2003).

[11] T.B. Anderson et al., ISS-CREAM Collaboration, *The ISS-CREAM Boronated Scintillator Detector, Proc. of the 33rd Int. Cosmic Ray Conf. 2013,* Rio de Janeiro, Brazil.

[12] EJ-200 and EJ-254 plastic data sheets. Eljen Technologies http://eljentechnology.com.

[13] Hamamatsu R1924A data sheet. https://www.hamamatsu.com/us/en/product/type/R1924A/index.html

[14] T.B. Anderson et al., *Design of a Gated-Dynode Photomultiplier Tube Assembly for the Boronated Scintillator Detector of the ISS-CREAM Experiment*, will appear in *Nucl. Inst. and Meth. A* 2019.

[15] T.B. Anderson, *Exploring the Cosmic Ray Spectrum with the CREAM Experiment*, Ph.D. Thesis, Penn State University (2013) https://inspirehep.net/record/1418241/files/Thesis-2013-Anderson.pdf

[16] L.M. Bollinger and G.E. Thomas, *Measurement of the Time Dependence of Scintillation Intensity by a Delayed-Coincidence Method, Rev. Sci. Instr.* 32 (1961) 1044. Erratum: *Rev. Sci. Instr.* 34 (1962) 497.

[17] J.G. Pronko, J.L. Guttman, G.A. Burginyon, and B. Jacoby, *Absolute Fluorescence Yields of Long and Short Term Decay Components of Selected Scintillators, Nucl. Inst. and Meth. A* 332 (1993) 121.